



## Investigation of photocatalytic activity of synthesized zinc stannate for tetracycline antibiotic degradation: modelling and optimization through RSM, ANN and genetic algorithm

Samira Taherkhani<sup>a</sup>, Hossein Karimi<sup>b,\*</sup>, Farzaneh Mohammadi<sup>c</sup>,  
Mohammad Darvishmotevalli<sup>b</sup>, Bijan Bina<sup>c</sup>

<sup>a</sup>Department of Chemistry, Faculty of Science, University of Zanjan, Zanjan, Iran, email: taherkhani\_s@ymail.com

<sup>b</sup>Student Research Committee and Department of Environmental Health Engineering, School of Health, Isfahan University of Medical Sciences, Isfahan, Iran, Tel. +98 9162244423; emails: h.karimi.m90@gmail.com (H. Karimi), mohamad.darvish68@gmail.com (M. Darvishmotevalli)

<sup>c</sup>Department of Environmental Health Engineering, School of Health, Isfahan University of Medical Sciences, Isfahan, Iran, emails: Fm\_1363@hlth.mui.ac.ir (F. Mohammadi), Bbina123@yahoo.com (B. Bina)

Received 22 January 2019; Accepted 30 June 2019

### ABSTRACT

The present study aims at investigating the ability of the synthesized zinc stannate, especially its photocatalytic activity, for degradation of tetracycline (TC) antibiotic under UV light irradiation. The process is assessed by four independent variables including pH, reaction time, initial TC concentration and photocatalyst dosage where TC removal is considered the response parameter. First, for optimization of the process, the response surface methodology (RSM) is implemented. Then, a second-order RSM model is developed based on experimental results. Subsequently, an artificial neural network (ANN) and a genetic algorithm are, respectively, applied for simulation and optimization of TC removal from aqueous solutions. Afterwards, an ANN model is trained by applying three different algorithms (scaled conjugate gradient, gradient descent and Levenberg–Marquardt algorithms), and the best algorithm is taken into account to develop a predictive model. Next, the optimal number of hidden layers is determined. Finally, to optimize effective input parameters and percentage of TC removal from aqueous solutions, the ANN model is used along with the genetic algorithm for the process optimization.

*Keywords:* Photocatalyst; Response surface methodology model; Artificial neural network model; Genetic algorithm; Tetracycline; Antibiotic

### 1. Introduction

Performance prediction of treatment plants is of particular importance due to the presence of emerging pollutants in water and wastewater. The computer simulation model is the best way for achieving this purpose. Artificial neural networks (ANNs) can be applied effectively to develop a water and wastewater treatment plant model containing

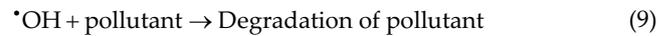
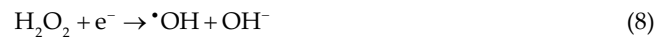
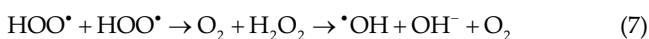
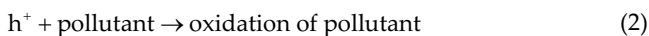
toxic pollutants [1,2]. One of the important kinds of emerging pollutants is antibiotics.

Antibiotics are broadly used in medicine and veterinary as pharmaceutical compounds for treating diseases and improving the overall health [3]. In terms of production and usage, tetracycline (TC) is one of the most important antibiotics used to treat infectious diseases. A considerable amount of these compounds enter aquatic ecosystems by

\* Corresponding author.

the pharmaceutical industry and after usage for household and hospital purposes. Such problems along with mismanagement would have side effects on human health [4,5]. Existence of TC causes toxicity and allergy in the environment and threatens human health [6,7]. Thus, elimination of pharmaceutical compounds such as TC antibiotic from aquatic environments is highly important. In recent decades, various methods have been used for the removal of pharmaceutical pollutants such as advanced oxidation processes (AOPs) [8,9], adsorption [10–12], filtration [13–15], chemical coagulation [16,17], etc.

Generally, an AOP includes all processes, in which active hydroxyl radicals are generated via various methods such as use of semiconductor oxides as a photocatalyst [18], which is called the photocatalytic degradation process. In this process, to destruct the organic pollutant, a photocatalyst (semiconductor) and a light source are needed. Zinc stannate (ZTO) is a semiconductor oxide that exists in the form of a nanoparticle. Having high surface area, appropriate size, and optical, electrical and catalytic properties related to their structure, nanoparticles have a great potential in being presented as a catalyst for water and wastewater processes [13]. ZTO is known as the most important trioxide semiconductor oxide. This semiconductor oxide has about 3.6 eV energy in a band gap. Moreover, having properties such as sustainability in all pHs and unique optical feature as well as electrical properties, ZTO is used as a photocatalyst for degradation of aquatic organic pollutants [19]. In previous studies, titanium dioxide anatase form was used in the presence of UV light to destruct TC [20]. Moreover, some methods used for degradation of TC from aqueous solutions include the following: ultrasound facilitates the dispersion of nanophotocatalyst  $\text{Bi}_2\text{Sn}_2\text{O}_7\text{-C}_3\text{N}_4$  over different amounts of zeolite for increasing solar light photocatalytic degradation of TC in aquatic environments [21], degradation of TC in water with  $\text{AMoO}_4$  photocatalysts [6], highly efficient visible-light photocatalytic activity of  $\text{Ag/AgIn}_3\text{S}_8$  for TC hydrochloride degradation [4], etc. In this study, a trioxide semiconductor oxide (i.e., ZTO) was used as it has the gap energy of 3.6 eV and also has better results than titanium dioxide (3.2 eV) in producing hydroxyl radicals in the presence of UV light. As ZTO has higher potentials in producing electrons, it would have a greater potential in degrading pollutants. The overall process taken place in the process of photocatalytic degradation is shown below:



The antibiotic properties of TC as a harmful and non-biodegradable contaminant are presented in Table 1.

Use of modelling combined with experimental studies has an important effect on cost and time saving. Some modelling methods such as ANN models or the response surface methodology (RSM) are well able to predict complicated processes. The performance of AOPs depends on various parameters such as oxidant and catalyst concentration and chemical structure, pH, UV dosage and type and energy applied in the process. These parameters also affect each other. The difficulty of modelling these processes is because of details of chemical reactions occurring in the system. For solving these systems, mass balance and energy equations must be applied, which is difficult and time-consuming. In this condition, using an ANN as a non-linear, fast and effective model could be considered [22].

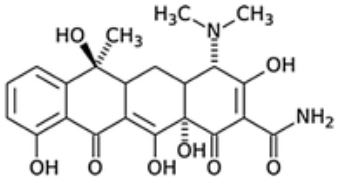
According to the literature, ANN modelling for AOPs, which contain nonlinear and complicated reactions between parameters, is highly applicable and effective [22–24].

Many researchers have implemented RSM for investigation and optimization of processes for water and wastewater treatment. As a constraint, RSM is unable to incorporate uncontrollable influential parameters. Alternatively, an ANN as a computer forecasting method assesses the function of the process through modifying weights of the network to yield the requisite target. It is noteworthy that this method does not present any information on the chemical/physical process influencing the system. Therefore, a robust non-parametric simulative model is developed. A number of comparative studies have been carried out on RSM with an ANN, implying that ANNs generate robust models with large correlation coefficients and lowest values of the mean squared error (MSE) [25].

Accordingly, an ANN-based model can investigate practical connections between response parameters and independent parameters (inputs) of a process by taking advantage of experimental data [26,27].

As a stochastic general search method, a genetic algorithm (GA) proceeds iteratively by producing new individual

Table 1  
Tetracycline antibiotic properties

Parameter	Property
Molecular formula	$\text{C}_{22}\text{H}_{24}\text{O}_8\text{N}_2\text{HCl}$
Molecular weight (g/mol)	480.9
Solubility (mol/L)	0.041
$\lambda_{\text{max}}$ (nm)	359
Chemical structure	

populations out of previous populations. A GA benefits from stochastic operators, namely crossover, mutation and selection, over an initially random selection so that a new population is computed. GAs are not identical to traditional optimization and search methods from four major perspectives:

GAs parallelly search within a population of response points. Thus, unlike traditional methods, they are able not to be trapped in local optimal points, thereby searching the best response points. Instead of using deterministic selection rules, GAs use probabilistic ones and focus on chromosome, an encoded form of potential parameters of solutions instead of parameters themselves. Without any other derivative or additional data, it also utilizes fitness scores obtained from objective functions [28,29].

The present study is aimed at investigating the photocatalytic degradation of TC antibiotic with ZTO nanoparticles under irradiation of UV light. Furthermore, we are intended to model the photocatalytic degradation process using RSM and ANN and optimize it with GA approach.

## 2. Materials and methods

### 2.1. Experimental design

The materials include TC antibiotic ( $C_{22}H_{24}O_8N_2HCl$ ), zinc nitrate hexahydrate and tin(IV) chloride pentahydrate with about 98% purity purchased from Sigma-Aldrich Co. as well as ammonia solution 32%, sodium hydroxide, and ethanol produced from Merck Co.

The following experimental instruments are used: the Shimadzu UV-visible spectrometer (model NO. 160A, Japan), the Heidolph MR 3001 K magnetic stirrer, the Metrohm Model 780 pH meter, an autoclave, a laboratory oven (Pars Azma Co.), a digital ultrasonic cleaner (CD-4820), and an electric furnace (Sybron Co.), Thermolyne Type 1500, with an accuracy of  $+10^{-5}$ .

### 2.2. Zinc stannate (ZTO) synthesis

The synthesis steps of ZTO are as follows:  $SnCl_4 \cdot 5H_2O$  (1.5 mg) and  $Zn(NO_3)_2 \cdot 6H_2O$  (3 mg) are dissolved in double-distilled water (20 mL) separately. Next, sodium hydroxide (20 mL, 1 M) is added to an agitating solution of  $SnCl_4 \cdot 5H_2O$ , inchmeal. Then, by mixing the zinc nitrate and former solution together, white hybrid sediments are formed. The sediments are carried to autoclave at a temperature of about  $200^\circ C$ – $220^\circ C$  and remain there for a period of 48 h. In the next step, the sediments are filtered off and then well washed by a water/ethanol mixture. Finally, the sediments are dried at  $80^\circ C$  for 20 h.

### 2.3. Photocatalytic properties of the synthesized zinc stannate (ZTO)

The photocatalytic properties of ZTO are evaluated for degradation of TC antibiotic under irradiation of UV light (30W-UV-C). To this end, a 200 mL glass beaker (lab glass) is applied as a reactor and 100 mL of TC solution is added to it and agitated by a magnetic stirrer.

Sampling from the reactor is carried out within 0 to 100 min. The TC concentration in each sample is measured

by the spectrophotometer (359 nm wavelength). The following equation is used for removal rate determination.

$$\text{Removal degree\%} = \frac{C_0 - C_t}{C_0} \times 100 \quad (10)$$

where  $C_0$  denotes the initial concentration of TC and  $C_t$  stands for the TC concentration at the time  $t$ .

### 2.4. Data analysis

First, RSM is implemented to model the photodegradation performance of TC antibiotic with ZTO employing four independent variables, namely pH, initial TC concentration, photocatalyst dosage, and reaction time, where TC removal is considered the response parameter. RSM uses some experimental design procedures, the most important of which is the central composite design (CCD) where many experiments can be parallelly conducted. This approach is relatively efficient for at most five factors (30). The number of experiments is obtained by Eq. (11):

$$l^m + 2m + C \quad (11)$$

where  $m$ ,  $l$  and  $C$  denote the number of factors, levels, and center point replicates, respectively [30].

In the RSM procedure, for verification of the model adequacy, several techniques are used. Some of these techniques are residual analysis, scaling residuals, prediction of error sum of squares residuals and tests of lack of fit [31].

The results of CCD experiments are modelled using RSM to fit appropriate equations. Table 2 presents the independent variables and their levels in experiments along with RSM coded values. Eq. (12) explains how the second-order polynomial model could be fitted to the experimental data [25].

$$y = \beta_0 + \sum_{i=1}^k \beta_i X_i + \sum_{i=1}^k \beta_{ii} X_i^2 + \sum_{i=1}^k \sum_{i \neq j=1}^k \beta_{ij} X_i X_j + \varepsilon \quad (12)$$

Here,  $y$ ,  $\beta_0$ ,  $\beta_i$ ,  $\beta_{ii}$ ,  $\beta_{ij}$ ,  $X_i$ ,  $X_j$ ,  $\varepsilon$  and  $k$  represent the predicted values, intercept constants, linear constants, quadratic constants, interaction regression constants, error and number of variables studied, respectively.

The neural network structure consists of the following layers: The input layer is made up of independent variables, hidden layers, and an output layer made up of dependent variables. First, a feed forward back propagation neural network (FFBPNN) with topology 4:5:1 is examined to select the best learning algorithm. Three learning algorithms including scaled conjugate gradient (SCG), gradient descent (GD) and Levenberg–Marquardt (LM) algorithms are tested. Subsequently, the number of neurons in the hidden layer was optimized. The network was fed by the input and output experimental parameters; Table 3 gives the variable ranges.

Fig. 2 illustrates the overall design of an FFANN with input, output and different number of hidden layers with the BP algorithm. It should be noted that log-sigmoid and tan-sigmoid transfer functions are applied in the hidden layer, and linear transfer function is used for the output layer.

Table 2  
Variables levels applied in RSM through the CCD method

Parameters	Level				
	-2	1-	0	1+	2+
( $X_1$ ) pH	4.5	6	7.5	9	10.5
( $X_2$ ) ZTO	100	150	200	250	300
( $X_3$ ) TC	10	15	20	25	30
( $X_4$ ) Time	10	40	70	100	130

Table 3  
Experimental range applied in ANN

Type	Variables	Range
Input	Initial pH	4.5–10.5
	ZTO dose (mg/L)	100–300
	TC initial concentration (mg/L)	10–30
	Reaction time (min)	10–120
Output	TC removal (%)	11.8%–93.5%

The SCG, GD and LM algorithms contribute to the training of the ANN model. About 65 sets of experimental results applied for modelling the network and the inputs are divided stochastically into three subsets: training (70%), validation (15%) and test (15%). First, within the training phase, each neuron connection among layers receives stochastic weights. The errors back propagated and weights keep being modified until the minimal error is reached for the predicted values in comparison with experimental results. In the following, the validation and testing steps of the ANN are carried out. In validation step, a set of experiments were used to tune the parameters of the MLP, the validation set would be used to find the optimal number of hidden units or determine a stopping point for the back-propagation algorithm and represents the generalization and robustness of the network. Test set is some

experiments used only to assess the performance of a fully-trained MLP, the test step would be used to estimate the error rate after choosing the final model (MLP size and actual weights).

The variables are optimized through a GA after the development of ANN model. A GA is defined as optimization strategies that are developed on the basis of natural selection principles. This algorithm benefits from a set of represented stochastic solutions in a number of cases to solve the problems. Later, some operators are iterated until the convergence is reached. Indeed, the GA-based optimization strategy can be referred as a general optimization method that is independent from initial values for reaching the convergence. However, the required computational time is probably the most serious drawback. The GA development entails some specific steps including: setting of solutions (which is called chromosomes) represented by population, selecting fitness function that defines how fit individuals, selecting the most superior chromosomes, and genetically propagating selected parents, particularly mutation and cross over. These two operators are applied to generate new and enhanced chromosomes [28]. To simulate the process, both the neural network and the GA are applied within the MATLAB software. Fig. 2 depicts the optimized form of the ANN-GA modelling.

### 3. Results and discussion

#### 3.1. Evaluation of the synthesized zinc stannate (ZTO) characteristics

In Fig. 3, the FT-IR spectrum of the synthesized ZTO is presented in the 500–4,000  $\text{cm}^{-1}$  by the hydrothermal method. The FT-IR spectrum shows that ZTO is on the absorption peaks of 582; 646; 1,030 and 3,400  $\text{cm}^{-1}$ . The peaks of 582 and 646  $\text{cm}^{-1}$  return to ZnO and SnO, respectively. The peaks of 1,030 and 2,930  $\text{cm}^{-1}$  are associated with the symmetric and asymmetric tensile vibrations of Zn-O-Sn, respectively. The peak of 3,400  $\text{cm}^{-1}$  is associated with the tensile vibrations of -OH at ZTO level.

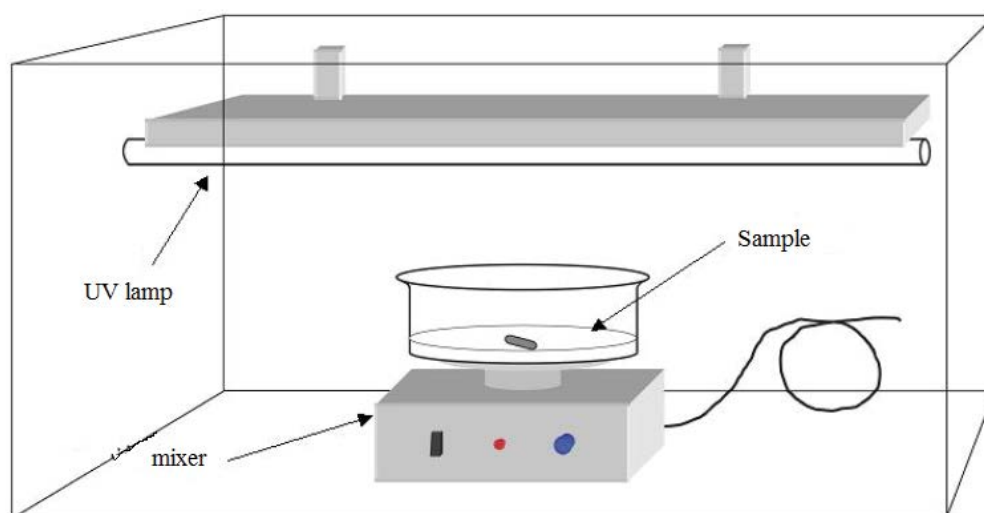


Fig. 1. The reactor of UV photoreactor schematically.

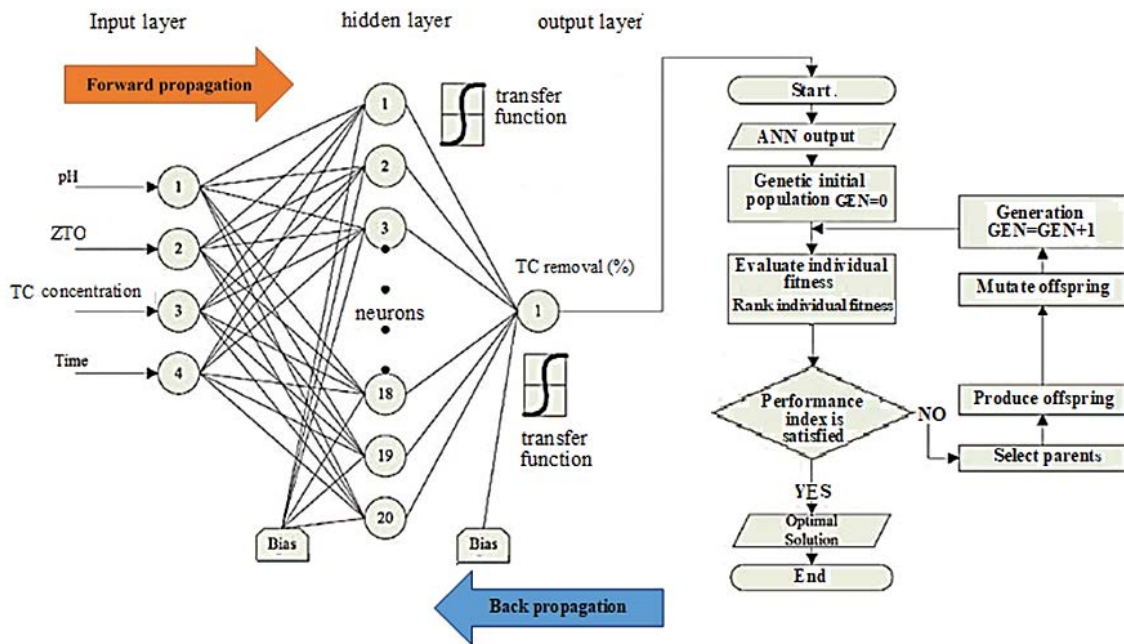


Fig. 2. Architecture of ANN–GA modelling.

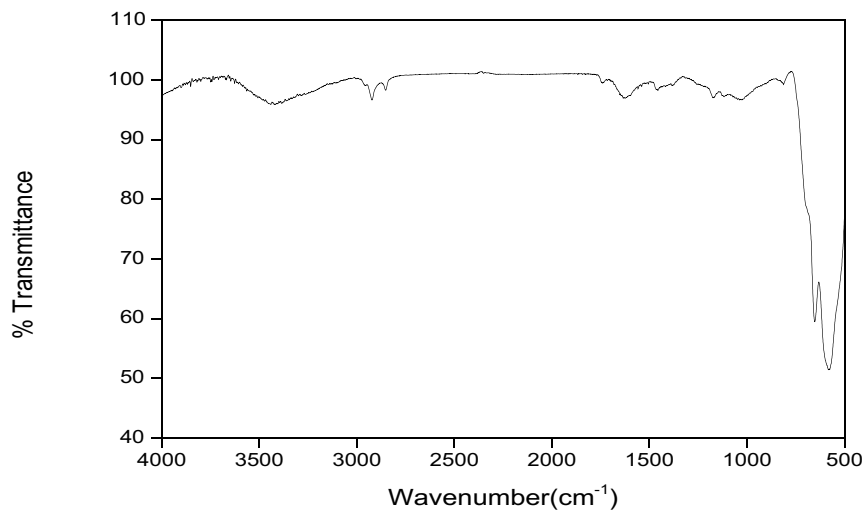


Fig. 3. FT-IR spectrum representation of synthesized ZTO.

In the photocatalyst structure, existing crystal phases (cart No: 2184-074-01) are determined by the location and relative magnitude of available peaks characterized with the X-ray diffraction pattern.

Fig. 5 shows the SEM images of the synthesized ZTO. It is found that the synthesized ZTO takes the shape of nanoflowers.

3.2. RSM modelling and optimization

Statistically designed experiments are conducted by applying CCD method to study how the independent variables affect TC removal. According to Fig. 6, the experimental results are drawn vs. predicted values with RSM model.

The fitted line is observed with a coefficient of correlation equal to 0.98, indicating the robustness of the model.

According to the observed data, a second-order polynomial model is developed by implementing RSM after deleting unimportant terms, as presented in Eq. (13):

$$\begin{aligned}
 Y = & 52.5714 - 30.6050(A) + 5.4833(B) - 3.5783(C) + 20.8317(D) \\
 & + 8.0806(A^2) - 7.0306(B^2) + 1.8694(C^2) - 9.1806(D^2) \\
 & - 13.1450(A \times B) - 2.5450(A \times C) + 1.3350(A \times D) - 1.3550(B \times C) \\
 & - 0.1350(B \times D) + 9.5650(C \times D) \quad (13)
 \end{aligned}$$

where Y, A, B, C and D stand for the degree of TC degradation, pH, photocatalyst dosage, initial concentration and

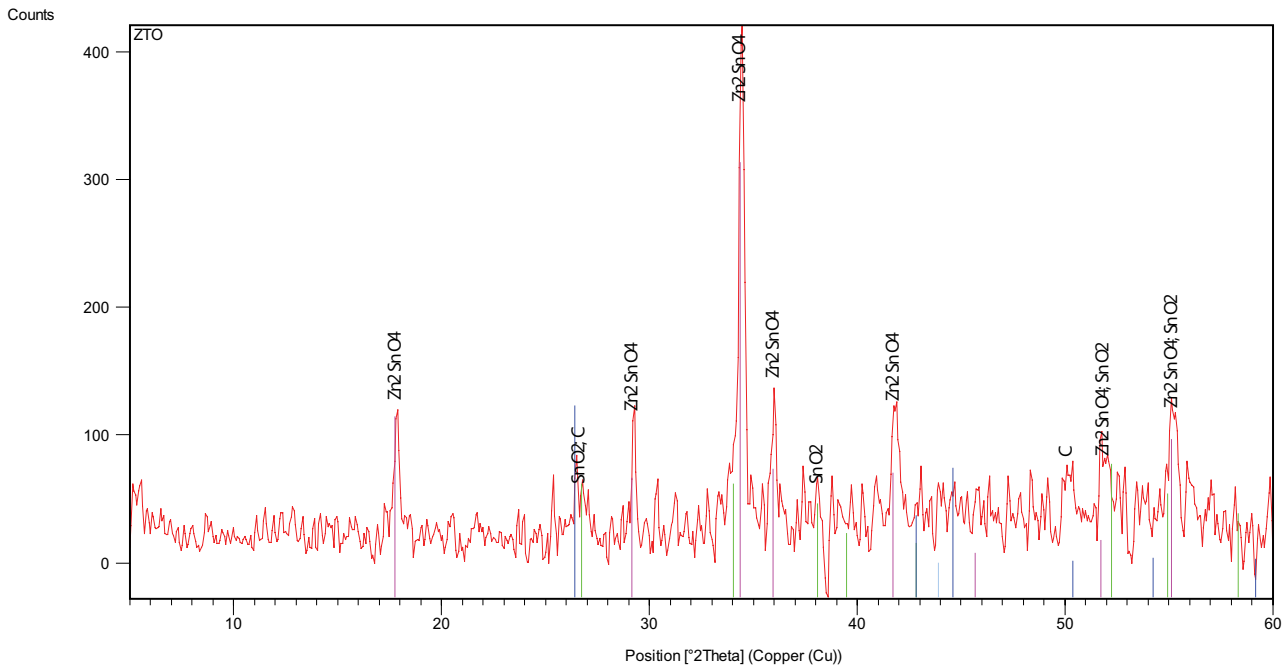


Fig. 4. X-ray diffraction (XRD) of synthesized ZTO.

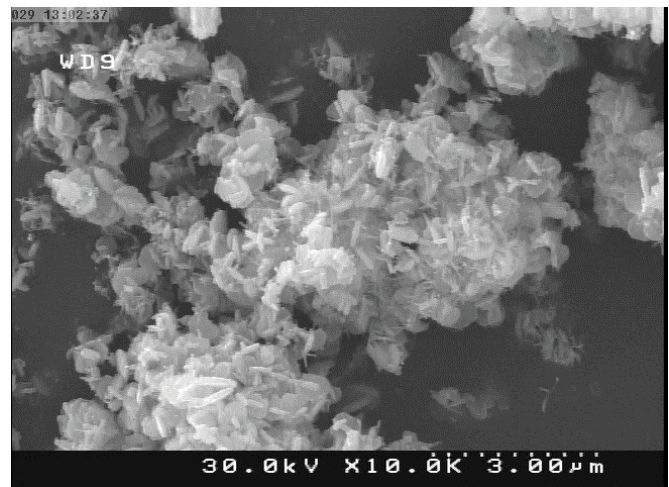
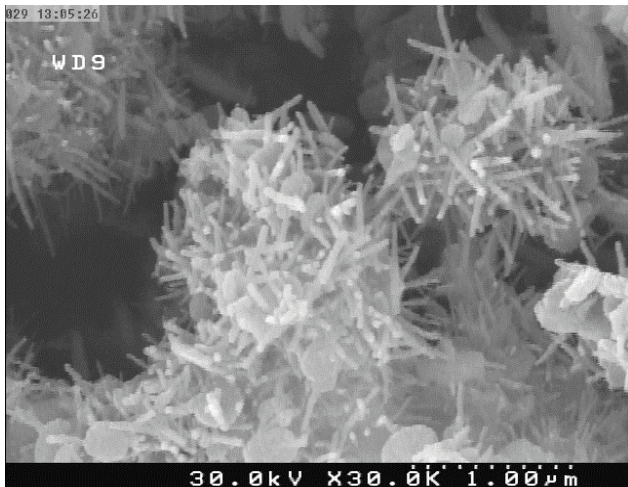


Fig. 5. SEM images of prepared ZTO.

reaction time, respectively. To assess the model, Table 4 gives the results obtained from the analysis of variance (ANOVA).

The Fisher test is conducted to analyze the statistical significance of the model. A low  $p$ -value indicates that the developed quadratic model is significant from a statistical perspective and can be applied for an accurate prediction of TC removal. Moreover, the results for  $p$ -value larger than 0.05 are not significant from a statistical perspective so that they can be deleted from the model unless they are complying with the model hierarchy. The large value of determination coefficient ( $R^2 = 0.9875$ ) for Eq. (13) implies the significance of the model and offers an appropriate correlation between the predicted and observed response values.

### 3.3. Effect of the experimental parameters on tetracycline (TC) removal

This paper investigates the effects of four different parameters, namely photocatalyst dosage, pH, reaction time and initial concentration of TC. It is necessary to optimize the photocatalyst dosage because it reveals the photocatalytic activity of ZTO for TC degradation and the treatment cost. Experiments are conducted at various factor levels and the analysis of obtained data is carried out using the Design-Expert software. It is obvious in Fig. 7a that the highest TC removal rate occurs at higher ZTO dosage. Furthermore, the TC removal rate increases by an increase in reaction time. After about 70 min, the removal rate exceeds 70% at

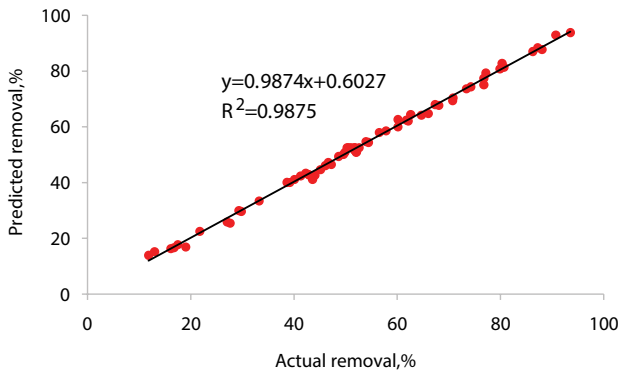


Fig. 6. The relationship between the predicted and actual responses.

Table 4  
ANOVA analysis for the selected quadratic model

Source	DOF	Adj SS	Adj MS	F-value	P-value
Regression	14	9,079.61	648.54	89.96	0.000
Residual	16	115.34	7.21	–	–
Total	30	9,194.96	–	–	–

SS: Sum of squares.

MS: Mean squares.

all initial concentrations. Moreover, Fig. 7 demonstrates that the highest removal rate occurs at the lowest pH (4.5) and any increase in pH imposes an adverse impact on photocatalyst activity within TC degradation. The highest rate of degradation occurs in the acidic environment because of the electrostatic attraction among the surface of the photocatalyst and pollutant. This is in a highly good agreement with reports presented in the literature [25]. Some reports

argued that the oxidation process was preferred within acidic environments [32,33]. All the samples exhibit a higher photodegradation at mild acidic pH, showing that the isoelectric point plays a central role in TC photodegradation [34].

Moreover, Fig. 7a illustrates how the initial TC concentration affects the removal efficiency. It is clearly evident that the initial TC concentration in a linear path has considerable effects on the removal efficiency. By increasing the initial TC concentration (10 to 30 mg/L) at constant ZTO dosage (200 mg/L) and pH (7.5) values, the TC removal efficiency decreases by about 20%. However, by increasing the reaction time, the TC removal percentage increases at all concentrations.

The pH associated with the photodegradation system is considered one of the most key parameters affecting the adsorption efficiency. Fig. 7b demonstrates a nonlinear relationship between the removal rate and pH. For ZTO nanoparticle, the surface charge changes by an increase in the values of pH and affecting the electrostatic properties of ZTO. It is clearly evident that an increase in pH affects the charge of the adsorbent surface and then causes decrease in the TC removal rate. Fig. 7c presents a nonlinear relationship between ZTO dosage and time vs. removal rate. It is visible that by increasing the reaction time and the ZTO dose, the removal rate is clearly increased. This point is also demonstrated in similar articles [34].

#### 3.4. Optimization of the process parameters

In this study, the optimum conditions are achievable for independent variables (initial pH, ZTO dosage, initial TC concentration and reaction time) and response parameter (TC removal rate) by extracting from the investigated levels. Here, it is aimed at maximizing TC removal while keeping other parameters “within the range”. All factors and responses receive the same weight. The TC removal

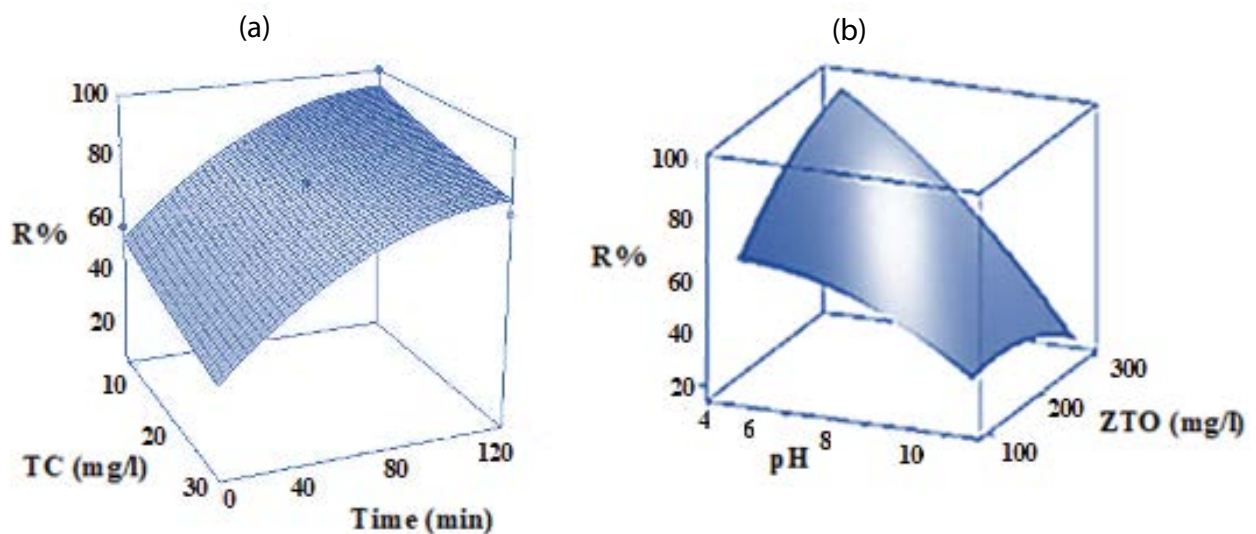


Fig. 7. Surface plots of photocatalytic destruction of TC. (a) Interaction effect of initial concentration and time on TC removal (at ZTO = 200 mg/L and pH = 7.5). (b) Interaction effect of pH and ZTO dosage on TC removal (at TC concentration = 20 mg/L and time = 70 min).

percentages of 79.0% and 93.54% are observed at the optimum values of ZTO dosage (250 mg/L), pH (4.5) and initial TC concentration of 10 and 30 mg/L, respectively. Furthermore, to validate the predicted results, confirmative experiments are performed at the optimum conditions. The predicted results offer a TC removal efficiency of  $77\% \pm 2\%$  and  $95.45\% \pm 2\%$  for the minimum and maximum initial concentrations, respectively. This suggests that the developed model is able to predict and optimize the TC removal process.

3.5. ANN model

For determining the TC removal rate, an ANN network is developed, as depicted in Fig. 2. First, a FFBPNN with the topology of 4:5:1 is examined to select the best learning algorithm. The tests are conducted on three learning algorithms including the SCG, GD and LM algorithms. The performance of the three mentioned algorithms is shown in Table 5. The correlation coefficient values (0.973, 0.978 and 0.981) and MSE values (0.304, 0.482 and 0.425) are calculated for the LM, GD and SCG algorithms, respectively.

As can be observed in Table 5, the LM algorithm is known with the acceptable *R* and low value of MSE. Based on the literature, the GD algorithm functions at a slow pace to converge the requisite value of the performance. The average time needed for network training by applying the LM algorithm is obtained minimum, while the maximum time is obtained applying the SCG descent algorithm [35]. Thus, to model TC removal, the LM algorithm is chosen and optimized to determine the suitable transfer function and number of neurons.

Three transfer functions, including tan sigmoidal, log sigmoidal and linear functions, would be investigated using the hidden layer neurons ranging from 5 to 20. Most researchers tested the number of neurons within the hidden layer ranging from 1 to 20 [36,37]. Nevertheless, the ANN performance will be directly affected by the number of hidden layers. The number of neurons should be sufficiently chosen, not so low that it cannot find the optimal function and not so high that it causes over fitting. The low number of neurons in hidden layers restricts the network over its training ability and capability of estimating results with desired accuracy [23,25]. Therefore, by comparing the efficiency of trained networks within a range of hidden layer neurons, the optimal number of hidden neurons is obtained.

The effectiveness of the ANN network topology and applicability of transfer function are well illustrated in Table 6. As can be observed, by increasing the number of neurons, the overall network performance also increases. It is observed that the minimum MSE and maximum correlation coefficient are obtained 0.023 and 0.996, respectively, for a network with 4:20:1 topology and tansig transfer function in hidden and output layers. This network is chosen as the best ANN model. Using an ANN, Gadekar and Ahammed [25] modelled dye removal through adsorption onto water treatment residuals. They investigated a variety of training algorithms and transfer functions. Above all, it is concluded that the LM training algorithm along with tansig transfer function provides the best performance.

The ANN-predicted and experimental values of TC removal are presented in Fig. 8 in all steps of the network validation. For evaluation of the network performance, the regression between the observed and predicted data is calculated and *R*<sup>2</sup> is calculated 0.992, tending to be 1. This certifies

Table 5  
Comparison of various training algorithms to predict TC removal

Description	Algorithm		
	Levenberg–Marquardt	Gradient decent	Scaled conjugate gradient
<i>R</i>	0.973	0.978	0.981
Mean square error (MSE)	0.304	0.482	0.425

Table 6  
Comparison of TC removal anticipation with application of different transfer functions and topologies

Topology	Transfer function					
	tansig		logsig		linear	
	MSE	<i>R</i> (all data)	MSE	<i>R</i> (all data)	MSE	<i>R</i> (all data)
4:5:1	0.304	0.973	1.125	0.865	3.26	0.74
4:10:1	0.118	0.981	0.751	0.945	1.44	0.792
4:15:1	0.091	0.97	0.184	0.893	0.967	0.865
4:16:1	0.086	0.975	0.089	0.964	1.12	0.88
4:17:1	0.097	0.854	0.096	0.939	0.892	0.754
4:18:1	0.057	0.905	0.042	0.961	0.827	0.932
4:19:1	0.035	0.985	0.043	0.964	0.746	0.957
4:20:1	0.023	0.996	0.034	0.981	0.637	0.969

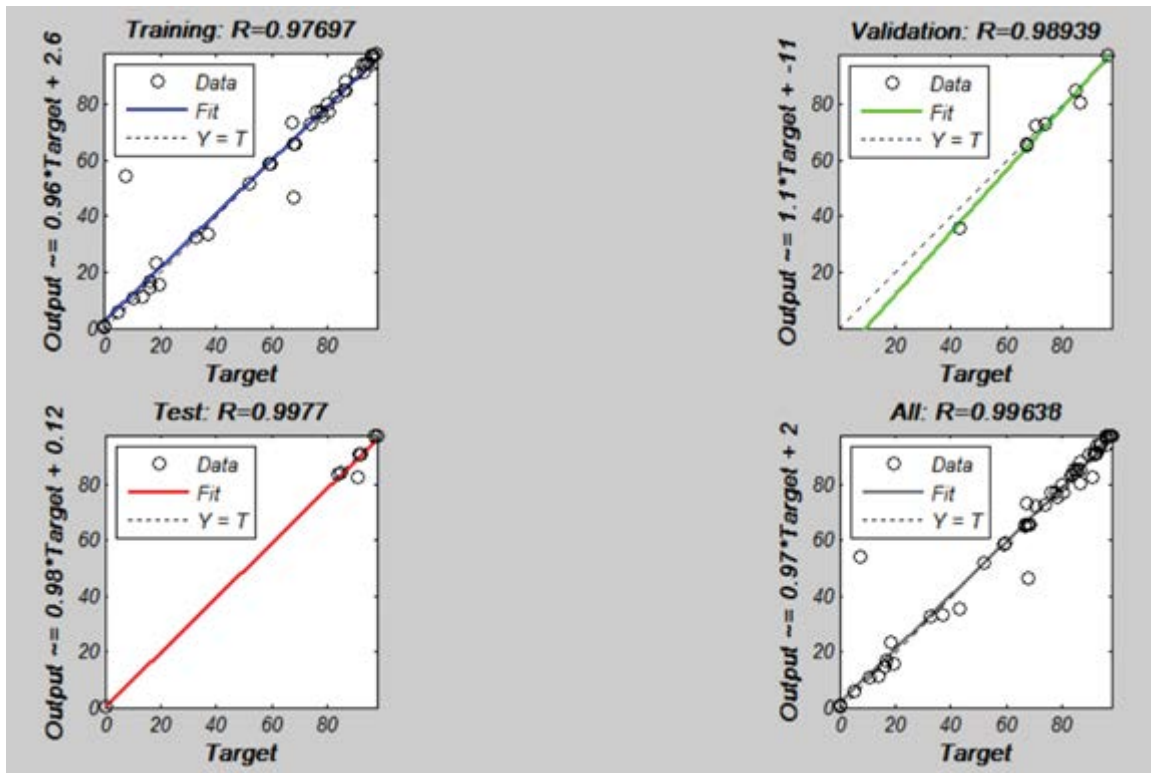


Fig. 8. Linear regression for observed and predicted data for TC removal by neural network.

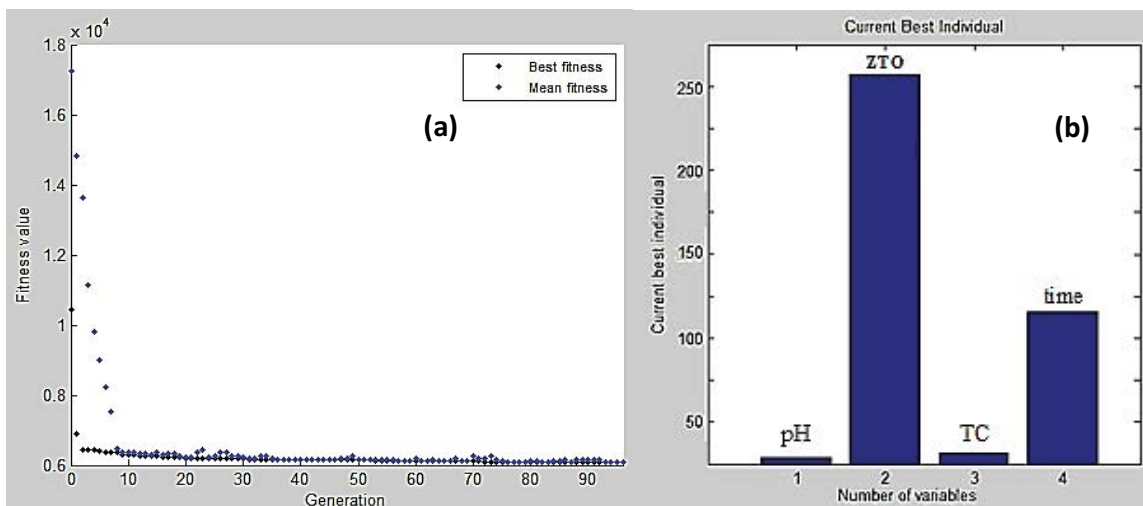


Fig. 9. GA output graphs.

the prediction accuracy by applying the developed trained ANN. Comparison of RSM with ANN models shows that the ANN  $R^2$  value is larger and is more in accordance with experimental data.

### 3.6. Genetic algorithm (GA) optimization

The developed neural network model is applied for optimization using the GA technique aiming at maximizing the percentage of TC removal from an aqueous solution.

The equation derived from the ANN model is applied as the objective function [38]:

$$\text{Objective function} = \text{tansig}(LW \times \text{tansig}(IW \times [X(1); X(2); X(3); X(4)] + b_1 + b_2) \tag{14}$$

where  $b_1$  and  $IW$  as well as  $b_2$  and  $LW$  stand for the bias and weights of the hidden layer as well as the bias and weights of the output layer, respectively.

The values of the GA-specific parameters incorporated in the optimization technique include number of generation 100, selection function of Stochastic uniform, the Rank scaling function, number of elite 2, crossover fraction of 0.8, and mutation function of constraint dependent and combination function of scattered. The optimum conditions are determined as follows: reaction time equal to 120 min, solution pH about 4.5, adsorbent dosage of 268 mg/L and TC concentration of 10.0 mg/L. Under these optimized conditions and by using GA, the model predicts the percentage of TC removal equal to 94.95%, where the experimental value is reported to be 93.54%, that is, the residual error between them is about 1.02%. This negligible error validates the constructed ANN-GA model. Fig. 9a shows the diagram of the best and average fitness values in each generation. Moreover, the best fitness value in the present generation is illustrated in Fig. 9b.

#### 4. Conclusion

This paper investigated TC removal from aqueous solutions by employing the photocatalytic activity of the synthesized ZTO. The experimental results were modelled and optimised using RSM, ANN and GA. The developed RSM model as the second-order polynomial model precisely provided the simulation of the impacts of the chosen variables on the process of antibiotic removal. The complex photocatalytic degradation process of TC with ZTO was modelled applying a multilayer (input, hidden and output layers) ANN. A tansigmoidal function was used at the hidden layer and a purlin was used at the output layer. Finally, a network with a topology of 4:20:1, MSE of 0.023 and R of 0.992 was selected as the best model. By implementing the LM algorithm, the ANN optimal topology was determined during the phase of training. The results revealed that a network with 20 neurons in the hidden layer offered the best performance. Based on the developed ANN model and by applying the GA procedure, the percentage of TC removal was favourably optimized. To this end, a maximal percentage of TC removal (94.95%) was obtained at the reaction time, solution pH, adsorbent dosage and TC concentration of 120 min, 4.5, 268 mg/L and 10.0 mg/L, respectively. Under the same conditions, the optimum experimental percentage of TC removal was reported 93.54%, that is, a residual error of about 1.02%.

#### Acknowledgements

The authors would like to express their gratitude to the Isfahan University of Medical Sciences (197094) for their financial support and assistance.

#### References

- [1] A. Aghaeinejad-Meybodi, A. Ebadi, S. Shafiei, A. Khataee, A.D. Kiadehi, Degradation of Fluoxetine using catalytic ozonation in aqueous media in the presence of nano- $\gamma$ -alumina catalyst: experimental, modeling and optimization study, *Sep. Purif. Technol.*, 211 (2019) 551–563.
- [2] L. Rossi, M. Bagheri, W. Zhang, Z. Chen, J.G. Burken, X. Ma, Using artificial neural network to investigate physiological changes and cerium oxide nanoparticles and cadmium uptake by *Brassica napus* plants, *Environ Pollut.*, 246 (2019) 381–389.
- [3] J.C. Sousa, A.R. Ribeiro, M.O. Barbosa, C. Ribeiro, M.E. Tiritan, M.F.R. Pereira, A.M.T. Silva, Monitoring of the 17 EU watch list contaminants of emerging concern in the Ave and the Sousa Rivers, *Sci. Total Environ.*, 649 (2019) 1083–1095.
- [4] F. Deng, L. Zhao, X. Luo, S. Luo, D.D. Dionysiou, Highly efficient visible-light photocatalytic performance of Ag/AgIn<sub>5</sub>S<sub>8</sub> for degradation of tetracycline hydrochloride and treatment of real pharmaceutical industry wastewater, *Chem. Eng. J.*, 333 (2018) 423–433.
- [5] F. Mohammadi, B. Bina, M.M. Amin, H.R. Pourzamani, Z. Yavari, M.R. Shams, Evaluation of the effects of Alkyl Phenolic compounds on kinetic parameters in a moving bed biofilm reactor, *Can. J. Chem. Eng.*, 96 (2018) 1762–1769.
- [6] A.M. Huerta-Flores, I. Juárez-Ramírez, L.M. Torres-Martínez, J.E. Carrera-Crespo, T. Gómez-Bustamante, O. Sarabia-Ramos, Synthesis of AMoO<sub>4</sub> (A = Ca, Sr, Ba) photocatalysts and their potential application for hydrogen evolution and the degradation of tetracycline in water, *J. Photochem. Photobiol., A*, 356 (2018) 29–37.
- [7] G. Islam, K. Gilbride, The effect of tetracycline on the structure of the bacterial community in a wastewater treatment system and its effects on nitrogen removal, *J. Hazard. Mater.*, 371 (2019) 130–137.
- [8] G.F. da Silva Brito, R. Oliveira, C.K. Grisolia, L.S. Guirra, I.T. Weber, F.V. de Almeida, Evaluation of advanced oxidative processes in biodiesel wastewater treatment, *J. Photochem. Photobiol., A*, 375 (2019) 85–90.
- [9] M.F. Khan, L. Yu, G. Achari, J.H. Tay, Degradation of sulfolane in aqueous media by integrating activated sludge and advanced oxidation process, *Chemosphere*, 222 (2019) 1–8.
- [10] P. Borthakur, P.K. Boruah, M.R. Das, N. Kulik, B. Minofar, Adsorption of 17 $\alpha$ -ethynyl estradiol and  $\beta$ -estradiol on graphene oxide surface: an experimental and computational study, *J. Mol. Liq.*, 269 (2018) 160–168.
- [11] J. Llado, M. Solé-Sardans, C. Lao-Luque, E. Fuente, B. Ruiz, Removal of pharmaceutical industry pollutants by coal-based activated carbons, *Process Saf. Environ. Prot.*, 104 (2016) 294–303.
- [12] S. Sessarego, S.C.G. Rodrigues, X. Ye, Q. Lu, J.M. Hill, Phosphonium-Enhanced Chitosan for Cr(VI) Adsorption in Wastewater Treatment, *Carbohydr. Polym.*, 211 (2019) 211–1.
- [13] S. Taherkhani, M. Darvishmotavalli, B. Bina, K. Karimyan, A. Fallahi, H. Karimi, Dataset on photodegradation of tetracycline antibiotic with zinc stannate nanoflower in aqueous solution-Application of response surface methodology, *Data Brief.*, 19 (2018) 1997–2007.
- [14] Y. Wang, H. Huang, X. Wei, Influence of wastewater pre-coagulation on adsorptive filtration of pharmaceutical and personal care products by carbon nanotube membranes, *Chem. Eng. J.*, 333 (2017) 333–1.
- [15] Y.-x. Zhao, P. Li, R.-h. Li, X.-y. Li, Direct filtration for the treatment of the coagulated domestic sewage using flat-sheet ceramic membranes, *Chemosphere*, 223 (2019) 383–390.
- [16] S.S.M. Hassan, H.I. Abdel-Shafy, M.S.M. Mansour, Removal of pharmaceutical compounds from urine via chemical coagulation by green synthesized ZnO-nanoparticles followed by microfiltration for safe reuse, *Arabian J. Chem.*, (2016) (In Press).
- [17] L. Shamaei, B. Khorshidi, B. Perdicakis, M. Sadzadeh, Treatment of oil sands produced water using combined electrocoagulation and chemical coagulation techniques, *Sci. Total Environ.*, 645 (2018) 560–572.
- [18] S. Sharma, V. Dutta, P. Singh, P. Raizada, A. Rahmani-Sani, A. Hosseini-Bandegharai, V.K. Thakur, Carbon quantum dot supported semiconductor photocatalysts for efficient degradation of organic pollutants in water: a review, *J. Cleaner Prod.*, 228 (2019) 228–310.
- [19] M. Rasoulifard, M.S. Dorraji, S. Taherkhani, Photocatalytic activity of zinc stannate: preparation and modeling, *J. Taiwan Inst. Chem. Eng.*, 58 (2016) 324–332.
- [20] R. Daghri, P. Drogui, Tetracycline antibiotics in the environment: a review, *Environ. Chem. Lett.*, 3 (2013) 209–227.
- [21] S. Heidari, M. Haghghi, M. Shabani, Ultrasound assisted dispersion of Bi<sub>2</sub>Sn<sub>2</sub>O<sub>7</sub>-C<sub>3</sub>N<sub>4</sub> nanophotocatalyst over various amount of zeolite Y for enhanced solar-light photocatalytic

- degradation of tetracycline in aqueous solution, *Ultrason. Sonochem.*, 43 (2018) 61–72.
- [22] T. Bolanča, Š. Ukić, I. Peternel, H. Kušić, A.L. Božić, Artificial neural network models for advanced oxidation of organics in water matrix—comparison of applied methodologies, *Indian J. Chem. Technol.*, 21 (2014) 21–29.
- [23] S. Dutta, S.A. Parsons, C. Bhattacharjee, S. Bandhyopadhyay, S. Datta, Development of an artificial neural network model for adsorption and photocatalysis of reactive dye on TiO<sub>2</sub> surface, *Expert Syst. Appl.*, 37 (2010) 37–12.
- [24] A. Hassani, A. Khataee, M. Fathinia, S. Karaca, Photocatalytic ozonation of ciprofloxacin from aqueous solution using TiO<sub>2</sub>/MMT nanocomposite: nonlinear modeling and optimization of the process via artificial neural network integrated genetic algorithm, *Process Saf. Environ. Prot.*, 116 (2018) 365–376.
- [25] M.R. Gadekar, M.M. Ahammed, Modelling dye removal by adsorption onto water treatment residuals using combined response surface methodology-artificial neural network approach, *J. Environ. Manage.*, 231 (2019) 241–248.
- [26] D.N. Kartic, B.C.A. Narayana, M. Arivazhagan, Removal of high concentration of sulfate from pigment industry effluent by chemical precipitation using barium chloride: RSM and ANN modeling approach, *J. Environ. Manage.*, 206 (2018) 69–76.
- [27] M.R. Sabour, A. Amiri, Comparative study of ANN and RSM for simultaneous optimization of multiple targets in Fenton treatment of landfill leachate, *Waste Manage.*, 65 (2017) 54–62.
- [28] F.S. Hoseinian, B. Rezai, E. Kowsari, The nickel ion removal prediction model from aqueous solutions using a hybrid neural genetic algorithm, *J. Environ. Manage.*, 204 (2017) 311–317.
- [29] Y. Yasin, F.B.H. Ahmad, M. Ghaffari-Moghaddam, M. Khajeh, Application of a hybrid artificial neural network–genetic algorithm approach to optimize the lead ions removal from aqueous solutions using intercalated tartrate-Mg–Al layered double hydroxides, *Environ. Nanotechnol. Monitor. Manage.*, 1–2 (2014) 2–7.
- [30] N. Arsalani, R. Nasiri, M. Zarei. Synthesis of magnetic 3D graphene decorated with CaCO<sub>3</sub> for anionic azo dye removal from aqueous solution: kinetic and RSM modeling approach, *Chem. Eng. Res. Des.*, 136 (2018) 136.
- [31] D.C. Montgomery. *Design and Analysis of Experiments*, John Wiley & Sons, 2017.
- [32] F.M. Bijan Bina, M.M. Amin, H.R. Pourzamani, Z. Yavari, Determination of 4-nonylphenol and 4-tert-octylphenol compounds in various types of wastewater and their removal rates in different treatment processes in nine wastewater treatment plants of Iran, *Chin. J. Chem. Eng.*, 26 (2018) 183–190.
- [33] Y. Liu, J. Kong, J. Yuan, W. Zhao, X. Zhu, C. Sun, J.M. Xie, Enhanced photocatalytic activity over flower-like sphere Ag/Ag<sub>2</sub>CO<sub>3</sub>/BiVO<sub>4</sub> plasmonic heterojunction photocatalyst for tetracycline degradation, *Chem. Eng. J.*, 331 (2018) 242–254.
- [34] J. Jeong, W. Song, W.J. Cooper, J. Jung, J. Greaves, Degradation of tetracycline antibiotics: mechanisms and kinetic studies for advanced oxidation/reduction processes, *Chemosphere*, 78 (2010) 533–540.
- [35] S. Tiwari, R. Naresh, R. Jha, Comparative Study of Back-propagation Algorithms in Neural Network Based Identification of Power System, *IJCSIT*, 5 (2013) 93–107.
- [36] R.R. Karri, M. Tanzifi, M. Tavakkoli Yarak, J.N. Sahu, Optimization and modeling of methyl orange adsorption onto polyaniline nano-adsorbent through response surface methodology and differential evolution embedded neural network, *J. Environ. Manage.*, 223 (2018) 517–529.
- [37] P.R. Souza, G.L. Dotto, N.P.G. Salau, Artificial neural network (ANN) and adaptive neuro-fuzzy interference system (ANFIS) modelling for nickel adsorption onto agro-wastes and commercial activated carbon, *J. Environ. Chem. Eng.*, 6 (2018) 7152–7160.
- [38] C. Sutherland, A. Marcano, B. Chitto, Artificial neural network-genetic algorithm prediction of heavy metal removal using a novel plant-based biosorbent banana floret: kinetic, equilibrium, thermodynamics and desorption studies, *Desal. Wat Treat.*, (2018).